Author(s): Stadler, Paul A.; Dodds, Stephen J.; Wild, Harald G.
Title: Observer based robust control of a linear motor actuated vacuum air bearing
Year of publication: 2007
Citation: Stadler, P.A.; Dodds, S.J.; Wild, H.G. (2007) 'Observer based robust control of a linear motor actuated vacuum air bearing' Proceedings of Advances in Computing and Technology, (AC&T) The School of Computing and Technology 2nd Annual Conference, University of East London, pp.212-221
Link to published version:
http://www.uel.ac.uk/act/proceedings/documents/ACT07.pdf

OBSERVER BASED ROBUST CONTROL OF A LINEAR MOTOR ACTUATED VACUUM AIR BEARING

Paul A. STADLER†, Stephen J. DODDS‡, Harald G. WILD†
†Institute for Mechatronic Systems, University of Applied Sciences Berne, Switzerland
‡University of East London, United Kingdom
paul.stadler@bfh.ch, s.j.dodds@uel.ac.uk, harald.wild@bfh.ch

Abstract: A vacuum air bearing based linear drive is to be positioned with a relative accuracy in the nanometer range. This is achieved by use of the new control technique, observer based robust control (OBRC) originated by the second named author and its motion control application published here for the first time. It is shown that the amplitude of the vibration mode of the vacuum air bearing excited by motion of the air molecules in the vacuum air bearing can be reduced from ±20nm (using a cascaded controller) to ±10nm using OBRC. Comparisons are made between simulations and experiments.

1. Introduction:

The work presented here is based on a vacuum air bearing based linear drive actuated by a voice coil motor that is to be positioned with a relative accuracy in the nanometer range. This high position accuracy is needed in applications such as wafer inspection systems in the semiconductor industry. Conventional bearings are said to stabilize the slider in ±1nm region (Cassat et. al., 2003) but it is known that this is a relative accuracy along a contorted path with lateral variations often extending to micrometers due to manufacturing imperfections. The vacuum air bearing of this paper exhibits this effect to a much lesser degree and is positioned using the new control technique 'Observer Based Robust Control' (OBRC), originated by the second author.

A diagram of the test rig is shown in Fig. 1. The slider has a vertical and a lateral guidance which are both pre-stressed due to pressurised air flowing out into thin channels (not shown) giving lift off and a vacuum inside a pocket of the channel pulling the slider back onto the surface, the neutral position where these forces are equal and opposite leaving a gap of about 3 microns. Previous work has shown that the vacuum air bearing suffers from a rotational oscillatory mode about the vertical axis at the centre of rotation (CR in Fig. 1) (Stadler et. al., 2005) and this has been found to limit the positioning performance of the test rig to about ±20nm. Therefore, the axis of action of the voice coil motor is displaced from the point, CR, to enable simultaneous control of the position and the oscillation angle, which should ideally be damped to zero. In Fig.1 the lateral bearing is shown, together with the mass-spring-damper model (Stadler et. al., 2005). Results using sliding mode control (SMC) were promising and allowed a positioning performance in the region of ±10nm (Stadler et. al., 2006). Further hardware improvements on the test rig led to an even better accuracy: below ±10nm. The motivation of using the new OBRC is due to the robustness that can be achieved not only against parameter variations but also model order uncertainty which cannot be accommodated by SMC, where the rank of the plant has to be known in advance (Vittek and Dodds, 2003).

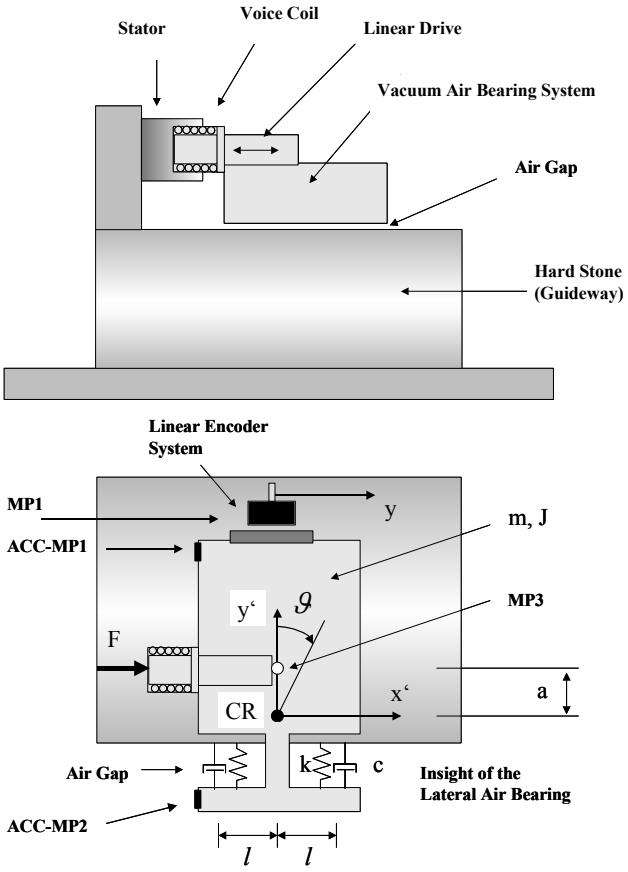

Fig. 1. Diagram of the vacuum air bearing based linear drive and its model.

2. Observer Based Robust Control:

The new control technique Observer Based Robust Control (OBRC), an invention of the second author, is used to control the position of a vacuum air bearing based linear drive. In (Stadler et. al., 2005) a linear state feedback control law supported by an observer similar to that of Fig. 2 is used which features estimation and compensation for an external disturbance, d, thereby preventing steady state errors with a constant reference input, y_r.

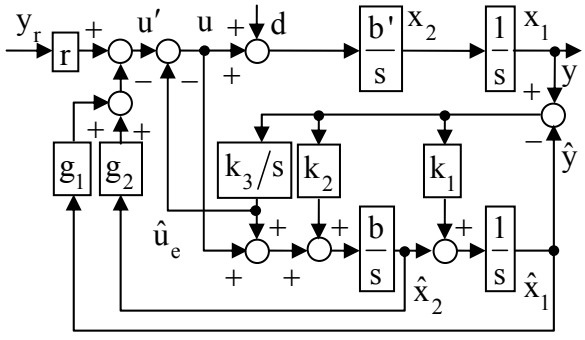

Fig. 2. Control of double integrator with external disturbance estimation, $\hat{u}_e \cong d(t)$, and compensation.

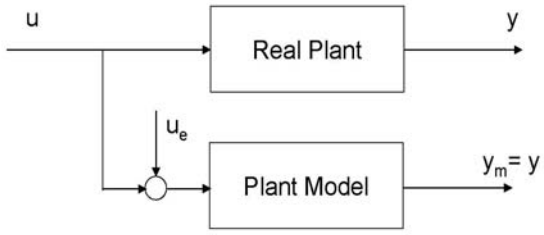

Fig. 3. Control variable difference $u_e(t)$ driving $y_m=y$.

This is achieved by treating d as a state variable with model, $\dot{d} = 0$, which, despite the assumption of constant d, allows time varying d to be estimated with minimal dynamic lag if the observer correction loop settling time is sufficiently short (equivalent to sufficiently high eigenvalues).

OBRC was inspired by this control system structure after it was found to exhibit robustness properties regarding parametric mismatching. The premise upon which OBRC is based is illustrated in Fig. 3.

It states that there exists an additional input, u_e, such that the output, y_m, of the plant model is equal to the output, y of the real plant. Now with reference to the observer in Fig. 2, the three model correction loop branches via the gains, k_1, k_2 and k_3, are equivalent to a single correction loop controller between the error, $e = y - \hat{y}$, and $\hat{u}_e$ acting at the model input, having transfer function $\frac{\hat{u}_e(s)}{e(s)} = G_{cl}(s) = k_1 s + k_2 + \frac{k_3}{s}$. Then the observer has the general structure shown in Fig. 4. Comparison with Fig. 3 then reveals that in the ideal observer where $e = 0$, then $\hat{u}_e = u_e$. This means that if the real plant is unknown, then, in principle, an *arbitrary* plant model could be taken and if the correction loop controller was able to drive the error, e, to negligible proportions, then $\hat{u}_e$ would be a good approximation to u_e.

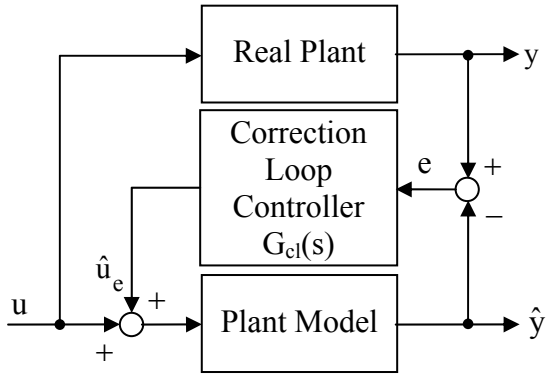

Fig. 4. Observer with correction loop controller.

To achieve this, the correction loop controller would require relatively high gains for the plant model to be allowed to differ considerably from the real plant. There should be no problem in achieving this as the correction loop would be closed around a known plant model and suitable design would guarantee its stability, but attention would have to be paid to the effects of measurement noise. Having achieved the estimation of u_e without accurate knowledge of the real plant, the crucial step in achieving a precisely specified closed loop dynamics is to let $u = u' - u_e$. Applying this to Fig. 3. yields Fig. 5.

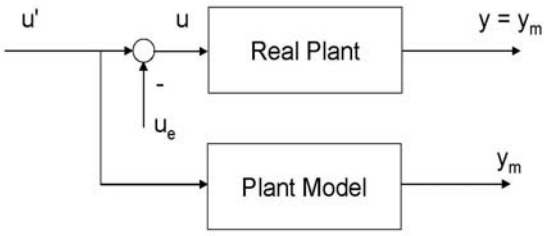

Fig. 5 Control variable difference $u_e(t)$ forcing real plant output to follow plant model output.

So the *unknown* real plant is forced to show the same input/output behaviour as the

known plant model and it is evident that this model can now be directly controlled by $u'(t)$. A state feedback controller can be used to yield the desired system behaviour, the control variable difference, $u_e(t)$, being estimated using an observer.

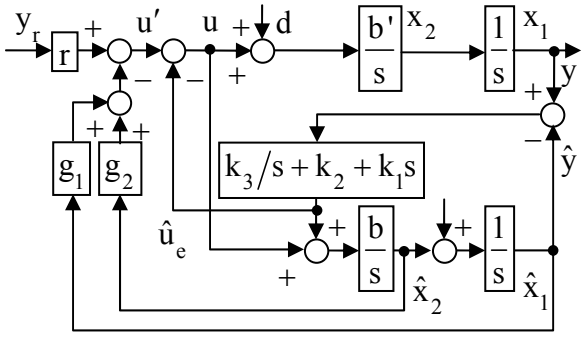

Fig. 6. Basic structure for OBRC for the double integrator plant. Note the PID-Structure of the observer correction loop involving k_1, k_2 and k_3.

Fig. 6 shows the resulting control system block diagram for the example of Fig. 2. In this case, $\hat{u}_e$ compensates for d and the difference between b and b′. It should be noted that the additional integrator of the observer with gain, k_3, is retained in order to avoid steady state errors with finite observer gains for step reference inputs. In this case,

$$\hat{u}_e(t) = \left(\frac{k_3}{s} + k_2 + k_1 s \right) \cdot e(t) \qquad (1)$$

and for a practical application, to avoid unacceptable amplification of the higher frequency components of measurement noise in $\hat{u}_e(t)$ the first derivative term is combined with a low pass filter with time constant T_f.

3. Derivation of the Observer Based Robust Control Law for the Test Rig:

The plant was modeled in (Stadler et. al., 2005) as a fourth order system and its state space model is:

$$\begin{cases} \dot{x}_1 = x_2 \\ \dot{x}_2 = \dfrac{k_a k_m}{m}(u - d) \\ \dot{x}_3 = x_4 \\ \dot{x}_4 = \dfrac{1}{J}\left(k_a k_m (u - d) a - 2l^2 k x_3 - 2cl^2 x_4 \right) \\ y = x_1 + R x_3 \end{cases} \qquad (2)$$

The states, x_1, x_2, x_3 and x_4, of the system are, respectively, the position, angle of rotation and angular velocity. The position measurement is then a weighted sum of x_1 and x_3, determined by the perpendicular distance between the control force vector and the centre of mass of the floating part of the rig. With reference to Fig. 1, the parameters are:

- Mass: m = 3.3 kg
- Moment of inertia: J = 30e-3 kg*m2
- Distance: a = 0.03 m
- Distance: l = 0.12 m
- Motor constant: km = 11.1 N/A
- Amplifier constant: ka =0.8 A/V
- Spring constant: k =29e5 N/m
- Damping constant: c =68 N/(m/s)
- Radius: R = 0.15m

Since the plant rank is 2, the observer model taken has the minimum of 2 integrators as in Fig. 6. Setting $b = 1$ was found sufficient. The derivation of the observer gains, k_1, k_2 and k_3, as well as the controller gains r, g_1 and g_2 is straight forward when using the Dodds settling time formula (Vittek and Dodds, 2003) to form the desired closed-loop dynamics:

$$T_s = \frac{3}{2}(n+1) \cdot T_c \qquad (3)$$

where T_s is the settling time (5% criterion) and the coincident closed loop poles are located at $-1/T_c$. Despite the plant order being four, its rank is 2 so y, is forced to follow $\hat{y}$, of the double integrator observer model and therefore

$$\frac{\hat{y}(s)}{y_r(s)} = \frac{r}{s^2 + g_2 s + g_1} = \left[\frac{\frac{3/2(1+n)}{T_s}}{s + \frac{3/2(1+n)}{T_s}} \right]_{|n=2}^{n} \quad (4)$$

so that

$$r = g_1 = \frac{81}{4T_s^2}, \quad g_2 = \frac{9}{T_s} \quad (5)$$

Similarly, the characteristic equation of the observer is

$$s^3 + k_1 s^2 + k_2 s - k_3 = 0 \quad (6)$$

and the desired characteristic equation yielding an observer correction loop settling time of T_{so} is given by

$$\left(s + \frac{3/2(1+n)}{T_{so}} \right)_{|n=3}^{n} = \left(s + \frac{6}{T_{so}} \right)^3 = 0 \quad (7)$$

Comparing equations (6) and (7) then yields

$$k_1 = \frac{18}{T_{so}}, \; k_2 = \frac{108}{T_{so}^2}, \; k_3 = \frac{216}{T_{so}^3} \quad (8)$$

where T_{so} is the settling time of the observer.

4. Simulations:

The simulations were carried out using Matlab/Simulink, including plant noise produced by the stochastic forces due to movements of air molecules in the vacuum air bearing. The level of this simulated plant noise was adjusted to yield similar stochastic variations of the measured position to those observed on the experimental rig on open loop.

The controller parameters are T_s=100ms, T_{so}=3ms; T_f=3ms, sampling frequency f_s=40kHz and λ=0.2.

A step response of 1μm is shown in Fig. 7 as well as a disturbance response after 0.5 seconds which is hardly visible despite the disturbance of 20mA being quite a harsh test on the nanometre scale. This can be seen when comparing the required positive and negative swing of the control variable for the 1μm step not being visible within the stochastic variations of the control variable that counteract the plant noise. The simulations are very promising as the position step response behaves as predicted by the settling time formula and the disturbance is rejected well.

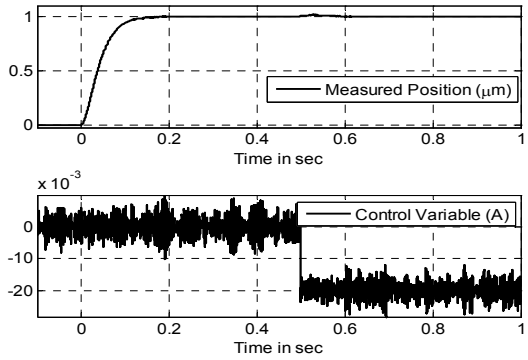

Fig. 7. Simulated step and disturbance response.

However, subsequent implementation of the control algorithm on the real time DSpace system showed a lower relative accuracy than predicted by the simulation. This was thought to be due to the relatively high value of k_3 and, in fact, an artificial scaling down of this gain by a factor, λ, was found to solve the problem, albeit with reduced disturbance rejection. The simulation is shown in Fig. 8.

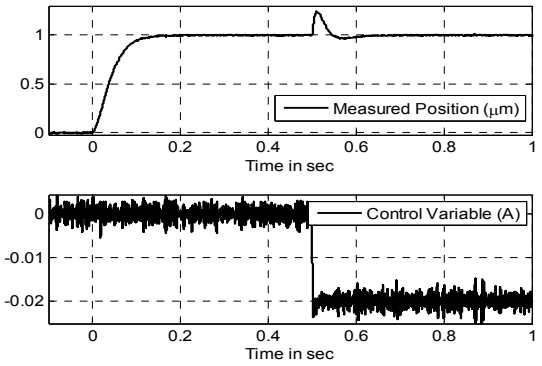

Fig. 8 Simulated step and disturbance response with k_3 scaling.

Besides the two low pass filters which had to be implemented in the paths after k_1 and k_2 used for the estimation $\hat{u}_e$ in the real time system, the last integrator of the observer is reset to the measured position upon initial loop closure (simulated by non-zero initial conditions) thereby preventing initial control saturation and consequent instability. In the real time system, the remaining two integrators were reset to zero at the same time.

The step response does not show any significant change when compared with the original simulation in Fig. 7 but the disturbance response now shows a maximum position deflection of about 250nm due to the imperfect $\hat{u}_e$: a compromise needed to attain high relative position control accuracy. Earlier results (Stadler et. al., 2006) using sliding mode control (SMC) exhibited a maximum deflection of 1.5μm and therefore the robustness using OBRC is still better than obtained with SMC. Introducing the λ scaling is certainly a compromise of the controller design for the time being, but it is possible to prove by means of a root locus that the system remains stable for all values of λ in the range $(0,1)$. Thus, the modified characteristic equation becomes:

$$s^3 + k_1 s^2 + k_2 s + k_3 \lambda = 0 \qquad (9)$$

For $K = (1-\lambda)/\lambda$, K varies between 1 and ∞ as λ varies between 1 and 0. For drawing the root locus one needs

$$K \cdot G(s) = -1 \Rightarrow K = -1/G(s) \qquad (10)$$

and with $\lambda = 1/(K+1)$,

$$k_3/(K+1) = -s(s^2 + k_1 s + k_2) \Rightarrow$$

$$K = \frac{-k_3}{s(s^2 + k_1 s + k_2)} - 1 = \frac{-k_3 - s(s^2 + k_1 s + k_2)}{s(s^2 + k_1 s + k_2)}$$

$$= \frac{-(s^3 + 3\frac{6}{Tso}s^2 + 3(\frac{6}{Tso})^2 s + (\frac{6}{Tso})^3)}{s(s^2 + k_1 s + k_2)}$$

$$= -(s + \frac{6}{Tso})^3 \Big/ \left[s(s^2 + k_1 s + k_2) \right]$$

Then KG(s) =-1, where $G(s) = \frac{s\left(s^2 + k_1 s + k_2\right)}{\left(s + 6/T_{so}\right)^3}$.

This is in the standard form for the root locus and it is straightforward to show that it lies in the left half of the s-plane for all K in the range $(0,\infty)$ and it follows that the system must be stable for λ in the range $(0,1)$.

5. Experimental Results:

Experimental results using the DSpace system are now presented. First, a step response of 1μm using a PI-P cascaded controller and an observer is shown in Fig. 9. This is designed by pole assignment assuming pure translational motion of the controlled rigid body with a settling time of 100ms and implementation with 40kHz sampling frequency, as for the OBRC, to allow a fair comparison. The undesired overshoot is due to the zero introduced by the controller in the closed loop transfer function.

Fig. 10 shows the disturbance rejection performance for later comparison with

OBRC. Next, stochastic performance is assessed with zero reference position. Fig. 11 indicates a peak error of about ±20nm.
In Fig. 12 good agreement with the simulation of Fig. 7 is evident. The small offset of about

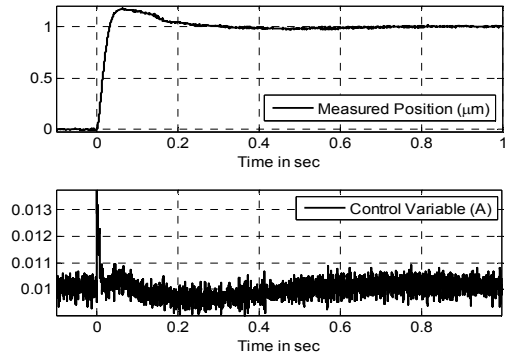

Fig. 9. Experimental 1 μm step response using a PI-P cascaded controller.

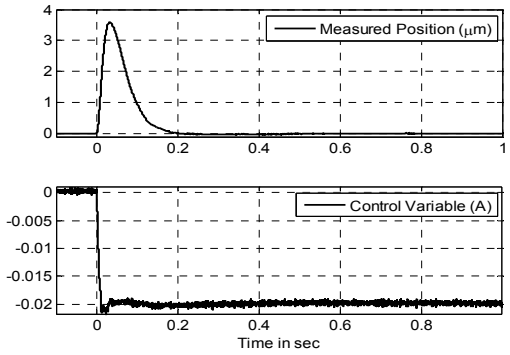

Fig. 10. Experimental 20mA step disturbance response using a PI-P cascaded controller.

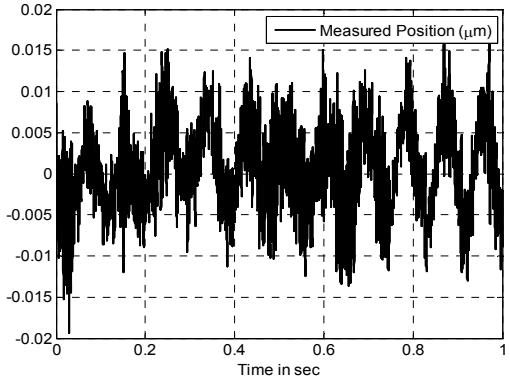

Fig. 11. Static measurement of the position using a PI-P cascaded controller.

5mA in the control variable is attributed to external forces from the wiring and tubing, gravitational forces due to a small inclination of the rig and magnetic forces from the motor stator, all acting on the slider.
Fig. 13 shows the measured position response to a 20mA disturbance step, having a maximum deflection of about 200nm, which is of the same order as predicted by the simulation, i.e., 250nm [Fig. 8]. Comparing this with Fig. 10 for the same test disturbance shows greatly improved disturbance rejection than that attained with the PI-P cascade controller. It also compares favourably with earlier investigations using other model based control strategies (Stadler et. al., 2005) and (Stadler et. al., 2006).

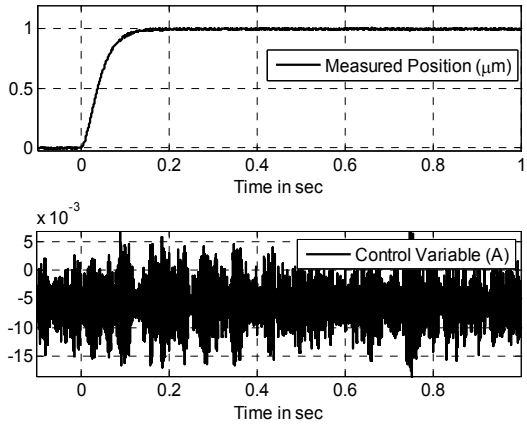

Fig. 12. Experimental 1 μm step response with OBRC.

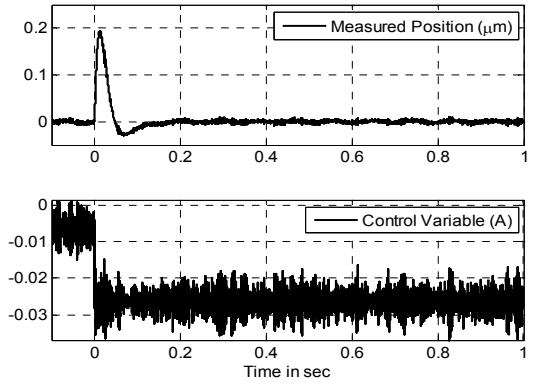

Fig. 13. Experimental 20mA step disturbance response with OBRC.

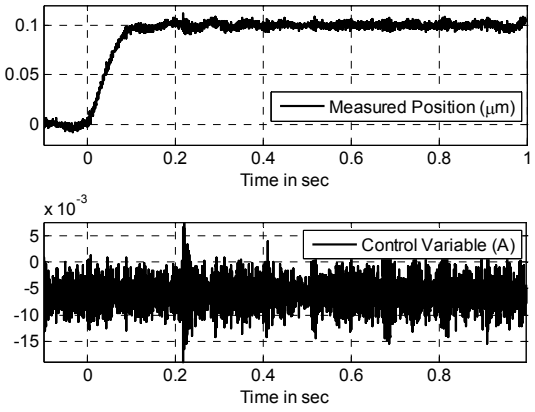

Fig. 14. Experimental 100nm step response with OBRC.

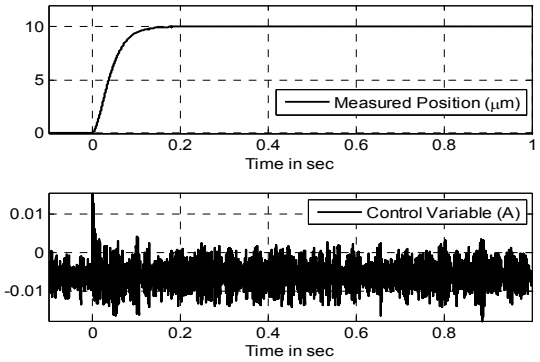

Fig. 15. Experimental 10μm step response with OBRC.

Further experimental step responses of 100nm and 10μm are shown in Fig. 14 and Fig. 15 again indicating the same second order behaviour as predicted using the

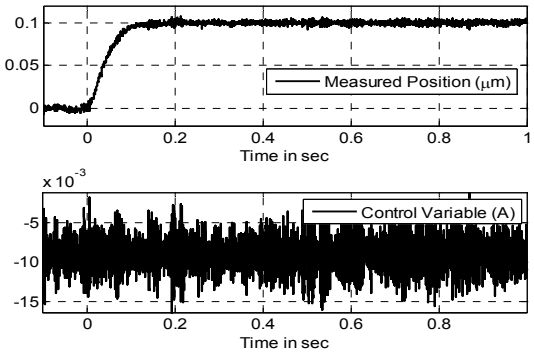

Fig. 16. Experimental 100nm step response with OBRC and added mass balanced about the centre of rotation.

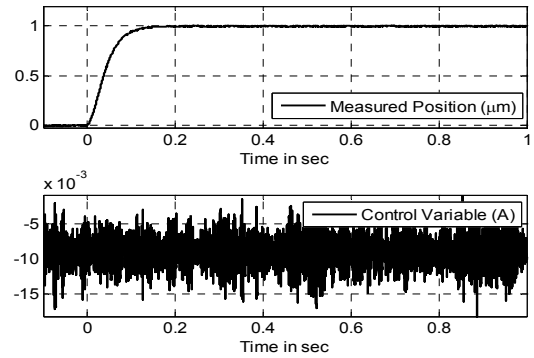

Fig. 17. Experimental 1 μm step response with OBRC and added mass balanced about the centre of rotation.

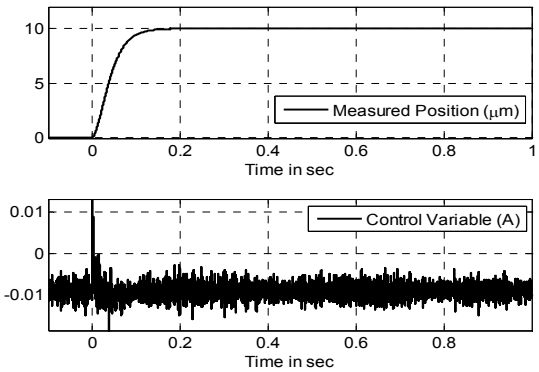

Fig. 18. Experimental 10μm step response with OBRC and added mass balanced about the centre of rotation.

settling time formula and coincident poles. As neither the controller gain or observer gain determinations require knowledge of the mass of the slider, it is expected that

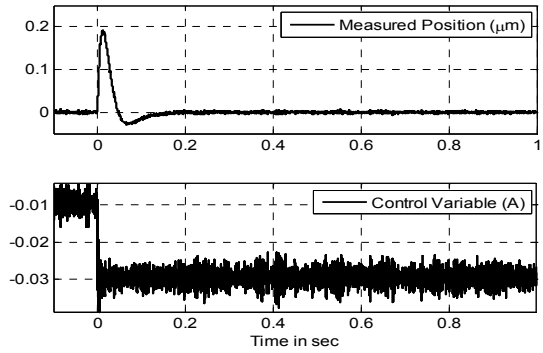

Fig. 19. Experimental 20mA step disturbance response with OBRC and added mass balanced about the centre of rotation.

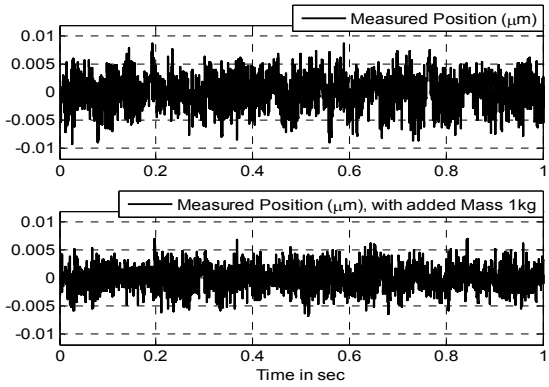

Fig. 20. Comparison of accuracies with OBRC with zero position reference.

when additional mass is added around the center of rotation of the rig, then the step responses should remain the same. This was put to the test by adding 1kg of extra mass to the slider and Fig. 16 to Fig. 18 show step responses which confirm the expected robustness of OBRC. Fig. 20 shows a relative accuracy within ±10nm and even below this when a mass of 1kg is added.

6. Conclusions and Recommendations:

The advantage of OBRC can be found in its straight forward design without the necessity of an accurate plant model, extreme robustness being implied. It must be born in mind, however, that an accurate plant model is still needed for simulations prior to implementation in specific applications. In this paper, the good performance of OBRC regarding realisation of the specified closed loop dynamics has been proven in simulations and experimental investigations on a vacuum air bearing based linear motor for high precision positioning of a slider achieving relative positioning accuracy in the nanometer range. In view of this, it is suggested that experiments are carried out to assess the positioning accuracy with time varying reference inputs and derivative feed-forward compensation to achieve nominally zero dynamic lag. The system also shows the robustness of OBRC despite the model in the observer being very different and simpler than the real plant. Further investigations are needed to find a way of ensuring closed loop stability during control saturation conditions. Since OBRC is not restricted to SISO plants. investigations of its performance with MIMO and nonlinear plants requires investigation.

7. References:

Cassat, A., Corsi, N., Moser, R. & Wavre, N., 'Direct Linear Drives: Market and Performance Status' *Proc. of the 4th Int. Symposium on Linear Drives for Industry Applications, Birmingham*, 2003, 1-11.

Stadler, P.A., Dodds, S. J. & Wild, H. G. 'Simultaneous High Precision Control of the Position and an Oscillatry Mode of a Vacuum Air Bearing Linear Drive'. *Proc.*

of the 5th Int. Symposium on Linear Drives for Industry Applications, Awaji, 2005, 116-119.

Stadler, P. A., Dodds, S. J. & Wild, H. G. 'Comparison of Nanometer Motion Control Techniques for Vacuum Air Bearings', *Proc. of International Control Conference (ICC 2006), Glasgow*, 2006.

Vittek, J. and Dodds, S. J., *Forced Dynamics Control of Electric Drives* (University of Zilina Press, 2003).